LOW-FREQUENCY $(OH)^-$ MOTIONS IN LAYER SILICATE MINERALS

by

A. W. NAUMANN, G. J. SAFFORD and F. A. MUMPTON

Union Carbide Corporation, Sterling Forest, Research Center, Tuxedo, New York

ABSTRACT

NEUTRON inelastic scattering spectra for kaolinite, dickite, pyrophyllite, and muscovite show a characteristic peak between 850 and 910 cm^{-1}, while those for chrysotile, antigorite, talc, phlogopite, and amphibole minerals show characteristic peaks at 620–650 cm^{-1} and 460–510 cm^{-1}. These peaks correspond to localized torsional oscillations of $(OH)^-$ groups. Lower-frequency peaks are also observed and are associated with optical and acoustic modes involving hindered translations. Within a series, the similarity in the shapes and the positions of the peaks indicates that the motions of the $(OH)^-$ groups are determined primarily by nearest-neighbor cation coordination. Differences between the two series can be attributed to the different environments when the octahedral layer of the lattice is populated either by two or by three cations.

The spectra of the hydrated minerals, montmorillonite, hectorite, and halloysite, show lines characteristic of liquid water. Upon dehydration, peaks corresponding to the motions of structural $(OH)^-$ units are observed.

INTRODUCTION

X-RAY diffraction and infrared (IR) absorption have been used extensively to study layer silicates, and have provided a fundamental knowledge of the crystal structures and of the bonding and coupling of their constituents. Polarized IR measurements have been particularly valuable in determining the orientation of $(OH)^-$ groups in certain of these minerals, have singled out vibrations involving hydrogenous units in normal and deuterated specimens and have differentiated between oscillatory and translatory vibrations (Farmer, 1958; Saksena, 1961; Stubican and Roy, 1961; Vedder and McDonald, 1963; Vedder, 1964). These studies have shown that the vibrations characteristic of $(OH)^-$ groups, considered as rigid units bound to a lattice, lie below 1000 cm^{-1}. These motions play an important role in understanding the bonding in layer minerals because they are the most sensitive to structural features such as the coordination between $(OH)^-$ groups and nearest-neighbor cations, the orientation of $(OH)^-$ groups relative to crystallographic axes, the extent of hydrogen bonding, and the strength of coupling between $(OH)^-$ groups and Si–O tetrahedral layers.

https://doi.org/10.1346/CCMN.1966.0140132 Published online by Cambridge University Press

Some clay minerals have been examined directly by IR in the region below 1000 cm^{-1} (op. cit.). Interpretation of these measurements is difficult, however, because not all frequencies of the vibrational modes are optically active, and others are not observed because measurements are seldom made below 400 cm^{-1}. In addition, many Si–O cooperative lattice modes have frequencies below 1000 cm^{-1}, complicating the spectra. Use has also been made of combination bands in the region of 3600 cm^{-1} that arise from the combination of low-frequency vibrations with the O–H stretching fundamental to give sum-and-difference side bands (op. cit.). However, IR and neutron scattering measurements on $Ca(OH)_2$, $Mg(OH)_2$, and LiOH have shown that difficulties are also encountered in analyzing this type of data (Safford, Brajovic, and Boutin, 1963; Safford and Lo Sacco, 1965). Not all low frequencies couple to the $(OH)^-$ fundamental to give observable side bands; in some cases, two sets of side bands may arise from a single vibrational mode; and it is sometimes difficult to determine whether a given peak is a side band, or a stretching mode that has been perturbed by weak hydrogen bonding or by the crystal field.

The neutron inelastic scattering (NIS) technique avoids a number of these problems. Frequencies down to approximately 8 cm^{-1} are readily measured; and they are observed directly, rather than as combination bands. By virtue of differences in scattering cross sections (Hughes and Schwartz, 1958), the most intense peaks are those associated with the vibrations of hydrogenous groups. Therefore, they are readily distinguishable from those of non-hydrogenous units. Finally, there are no selection rules; all the vibration frequencies are observed (Kothari and Singwi, 1959).

In this investigation, the vibrations of $(OH)^-$ groups from 1000 to 8 cm^{-1} in a series of di- and trioctahedral minerals have been compared by NIS. A systematic comparison of these motions in structurally related minerals has been made to correlate the binding characteristics of the $(OH)^-$ groups of these minerals with structural information.

The authors wish to express their gratitude to Dr. R. S. Hansen for helpful and informative discussions during the course of the work. They would also like to thank Mr. R. A. Morgan for his help in collecting data.

EXPERIMENTAL METHOD

All spectra were obtained using an inelastic neutron scattering spectrometer similar to those described previously (Eisenhauer, *et al.*, 1958). As shown schematically in Fig. 1, a beam of neutrons approximating a Boltzmann velocity distribution, is filtered through 12 in. of refrigerated, polycrystalline beryllium before impinging on a sample. Neutrons with energies less than the energy of the "Bragg cut-off" of Be are transmitted, while those of higher energies are scattered out of the beam. The filter serves three functions: (1) it produces a nearly monochromatic band of neutrons with an average energy of 4 ± 1 milli-electron volts (meV), an energy well below kT (25.3

https://doi.org/10.1346/CCMN.1966.0140132 Published online by Cambridge University Press

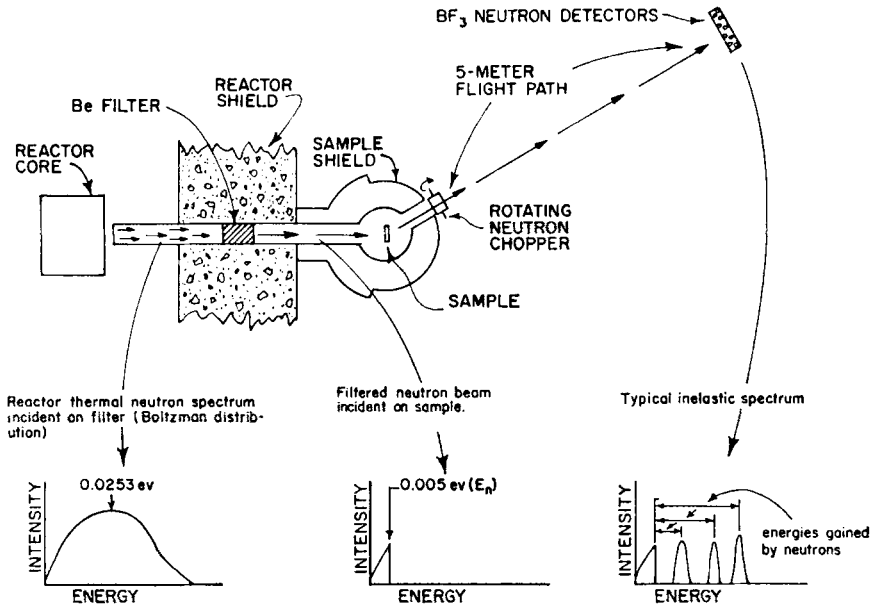


FIG. 1. Schematic of neutron inelastic scattering spectrometer.

meV) at room temperature; (2) it provides a sharp, high-energy edge at 5.2 meV corresponding to the "Bragg cut-off" for Be, providing an energy reference in the neutron spectra; and (3) it provides a "clean" region above 5.2 meV into which neutrons that have gained energy are scattered.

A neutron impinging on a sample may either gain or lose quantized units of energy corresponding to molecular vibrations. Because of (3) above, only energy gains are observed. The scattered neutrons are then chopped into bursts by a rotating collimator, and their velocities (hence, their energies) are determined by measuring their flight times over a 4.73-m flight path. These measurements yield best resolution in the region 900 to 8 cm^{-1}, comparable to the range observed by far-IR measurements.

The samples studied are listed and described in Table I. All were identified by X-ray diffraction and, unless otherwise indicated, were more than 90% pure. They were mounted in a 4 × 4 in. Cd shielded holder and were thin enough (usually $\approx$ 5 mm) to make multiple scattering negligible (Danner, *et al.*, 1964). All spectra were corrected for background, BF_3 neutron detection efficiency, and the transmission function of the chopper. Thus, the reported spectra are free of these instrumental effects.

EXPERIMENTAL RESULTS

Time-of-flight distributions are given in Figs. 2 to 7. The abscissae of these figures correspond to the time-of-flight of neutrons, as given by the number

https://doi.org/10.1346/CCMN.1966.0140132 Published online by Cambridge University Press

TABLE I.—DESCRIPTION AND IDENTIFICATION OF MINERAL SPECIMENS

Specimen	Locality	Description and remarks	State of aggregation
Chrysotile 1	New Idria, Cal.	Large, leathery sheet of matted chrysotile (short fiber)	Sheet
Chrysotile 2	Cassiar, Brit. Col.	Long fiber chrysotile asbestos, opened product	Filter cake
Chrysotile 3	Thetford, Quebec	Long fiber chrysotile asbestos, natural	Fibrous laths
Antigorite 1	Yukon Terr., Canada	Hard, dense, dark-green serpentinite, primarily antigorite, with some magnetite	10 × 40 mesh granules
Antigorite 2	Lancaster, Pa.	Hard, dense, dark-green serpentinite, primarily antigorite	10 × 40 mesh granules
Kaolinite 1	Dry Branch, Ga.	Premax Grade kaolin, Georgia Kaolin Co.	−325 mesh powder
Kaolinite 2	Tonopah, Nevada	Natural, unprocessed kaolinite	10 × 40 mesh granules
Dickite 1	Beaver Co., Utah	Dickite clay associated with alunite deposits	10 × 40 mesh granules
Dickite 2	Chihuahua, Mexico	Cream-colored clay, A.P.I. Ref. Clay No. 15	10 × 40 mesh granules
Talc 1	Gouveneur, N.Y.	White foliated cleavage fragments	10 × 40 mesh flakes
Talc 2	Holly Springs, Ga.	Green foliated masses	$\frac{1}{4}$–$\frac{1}{2}$ in. flakes
Pyrophyllite 1	Indian Gulch, Cal.	Acicular aggregates of pink laths	10 × 40 mesh laths
Pyrophyllite 2	Robbins, N.C.	Greenish-white sheets, A.P.I. Ref. Clay No. 49 (some kaolinite and muscovite present)	20 × 40 mesh laths
Phlogopite 1	Denholm Twp., Quebec	Brown sheet, asterated	Sheet
Phlogopite 2	La Tuque, Quebec	$\frac{1}{4}$ in. flakes, brown mica	Flakes
Muscovite 1	Effingham Twp., Ont.	Large book of white mica	Sheet
Muscovite 2	Eau Claire, Ont.	Large sheets of white mica	Sheet
Muscovite 3	Grafton, N.H.	Large sheets of white mica	Sheet
Halloysite	Bedford, Indiana	A.P.I. Reference Clay No. 12	10 × 40 mesh granules
Montmorillonite	Chambers, Arizona	A.P.I. Reference Clay No. 23	−100 mesh powder
Hectorite	Hector, California	White clay	−200 mesh powder
Crocidolite	South Africa	Cape Blue asbestos, 1–2 in. fibers	Fibers
Actinolite	Massachusetts	Green-bladed crystal fragments	10 × 40 mesh laths
Tremolite	Balmat, New York	Clear, crystal fragments	10 × 40 mesh granules
Anthophyllite	Bakersville, N.C.	Long, white fibers	Coarse laths and fibers

https://doi.org/10.1346/CCMN.1966.0140132 Published online by Cambridge University Press

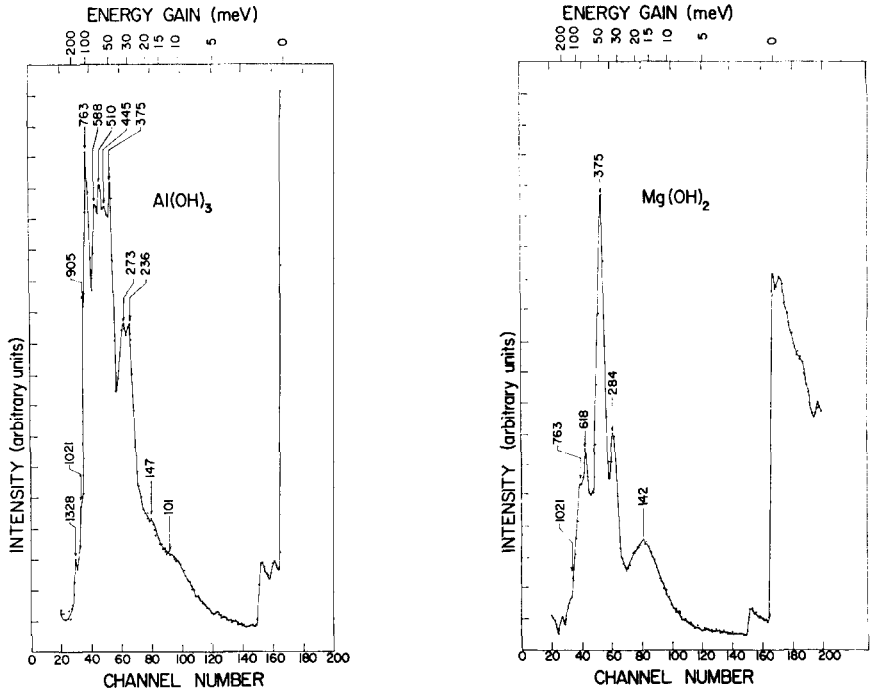


FIG. 2. Time-of-flight distributions for (a) aluminum hydroxide and (b) magnesium hydroxide.

of 28-microsecond channels. A scale for neutron energy gains in meV is given at the top of the figures, and the vibrational frequencies associated with the individual peaks of the spectra are indicated and identified in terms of wave numbers (cm^{-1}). The ordinates correspond to the corrected intensity of the scattered neutrons in arbitrary units. All samples were run to nearly equivalent statistics, then their spectra were normalized to give a common maximum intensity The sharp rise in the spectra starting at channel 165 conconstitutes the high-energy limit of elastic scattering from the sample and corresponds to the "Bragg cut-off" in beryllium at 5.2 meV. The small secondary peaks at about channel 150 are due to two partially resolved, secondary, "Bragg cut-offs" in beryllium at 6.8 and 6.5 meV. A summary and a comparison of the frequencies observed for the various samples are given in Table 2, and a comparison of some of these results with recent infrared data is given in Table 3.

Certain of the peaks of Figs. 2 to 7 may appear questionable, but this is due to a loss of resolution that accompanied the size reduction and reproduction of the original spectra. The solid lines of the figures were drawn through the data points, taking into account their statistical weighting. All of the peaks

https://doi.org/10.1346/CCMN.1966.0140132 Published online by Cambridge University Press

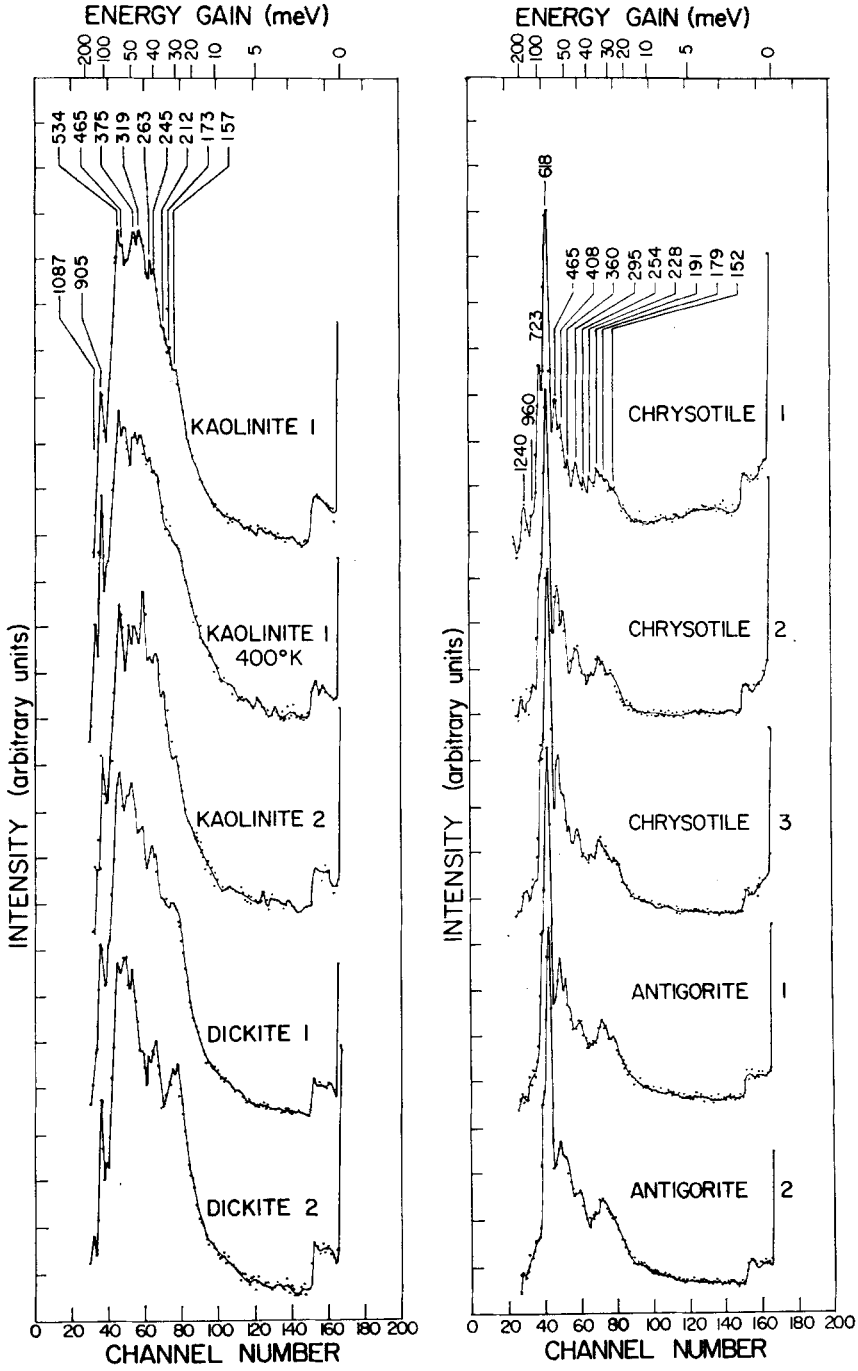


FIG. 3. Time-of-flight distributions for (a) kaolin and (b) serpentine specimens.

https://doi.org/10.1346/CCMN.1966.0140132 Published online by Cambridge University Press

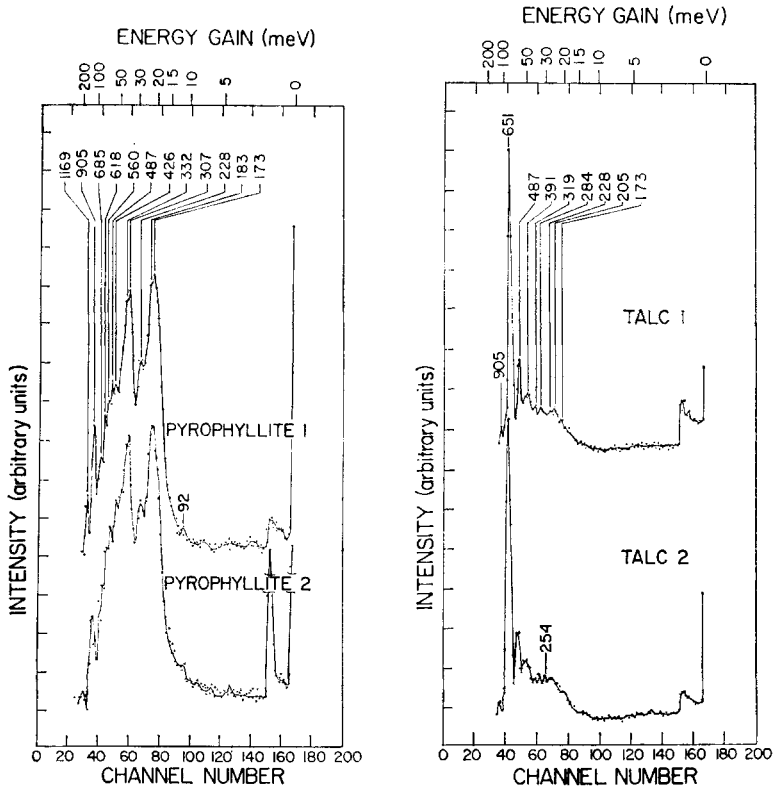


FIG. 4. Time-of-flight distributions for (a) pyrophyllite and (b) talc specimens.

indicated were outside of statistical uncertainty. The time-of-flight distributions were reproducible for a given sample with respect to both the frequencies and the relative intensities of the individual peaks. It was found, however, that when a given sample was ground finer than 200 mesh, its spectrum showed a broad and structureless rise in intensity below 150 cm^{-1}, and, in a few cases, the peaks in the 300–100 cm^{-1} range were slightly less well-resolved. As is shown in Table 1, this effect was avoided, except for inherently fine materials, by using samples of large particle size.

The time-of-flight distributions are arranged to show that a given mineral gives rise to a characteristic set of frequencies regardless of sample origin. This is particularly true for the trioctahedral layer minerals (Figs. 3b, 4b, and 5b) and the amphiboles (Fig. 6), which gave nearly identical spectra with regard to the frequencies, shapes, and relative intensities of the observed peaks, not only between different specimens of the same mineral type, but also between different minerals in the same group. In all cases, the dominant

https://doi.org/10.1346/CCMN.1966.0140132 Published online by Cambridge University Press

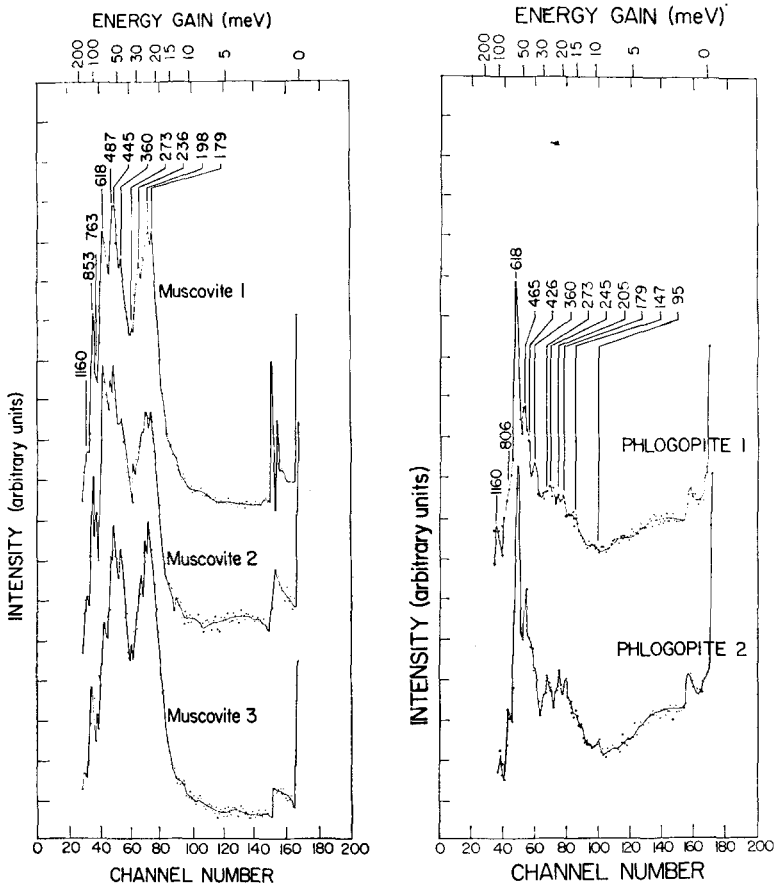


FIG. 5. Time-of-flight distributions for (a) muscovite and (b) phlogopite specimens.

features of the curves are a sharp primary maximum in the range 620–650 cm^{-1} and a secondary maximum in the range 460–510 cm^{-1}. In addition, there are a number of less intense, closely spaced frequencies in the range 400–150 cm^{-1}.

The spectra of the dioctahedral minerals (Figs. 3a, 4a, and 5a) differ considerably from those of their trioctahedral counterparts. Where a single maximum dominates the spectra for the latter, the former give rise to two or more major peaks. Again, there is a correspondence in the frequencies of peaks, both between specimens of the same mineral and between different minerals in the group. As shown in Table 2, there is also a correspondence with the frequencies observed for the trioctahedral minerals. In contrast, however, significant variations in peak intensities were found for dioctahedral

https://doi.org/10.1346/CCMN.1966.0140132 Published online by Cambridge University Press

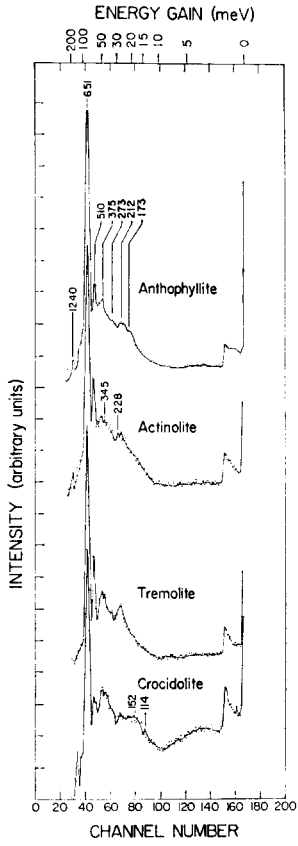


FIG. 6. Time-of-flight distributions for amphibole minerals.

mineral specimens from different localities, and even greater variations between different mineral types. A sharp peak of medium intensity in range 850–910 cm^{-1} appears in the spectra of all the dioctahedral minerals.

Time-of-flight distributions for liquid water and for hydrated and dehydrated halloysite, montmorillonite, and hectorite are given in Fig. 7. The spectra of the hydrated forms show lines characteristic of liquid water with a few of the more dominant structural $(OH)^-$ frequencies superimposed.* The specimens of halloysite and montmorillonite were the most highly hydrated, and gave spectra most like that of water. The hectorite specimen was less completely hydrated and shows structural $(OH)^-$ frequencies more distinctly. After dehydration by heating at 250°C for 18 hr, halloysite and

* It is of interest, in view of the results of Graham, Walker, and West (1964), that the interlayer water of the hydrated minerals has structure and bonding like that of liquid water.

https://doi.org/10.1346/CCMN.1966.0140132 Published online by Cambridge University Press

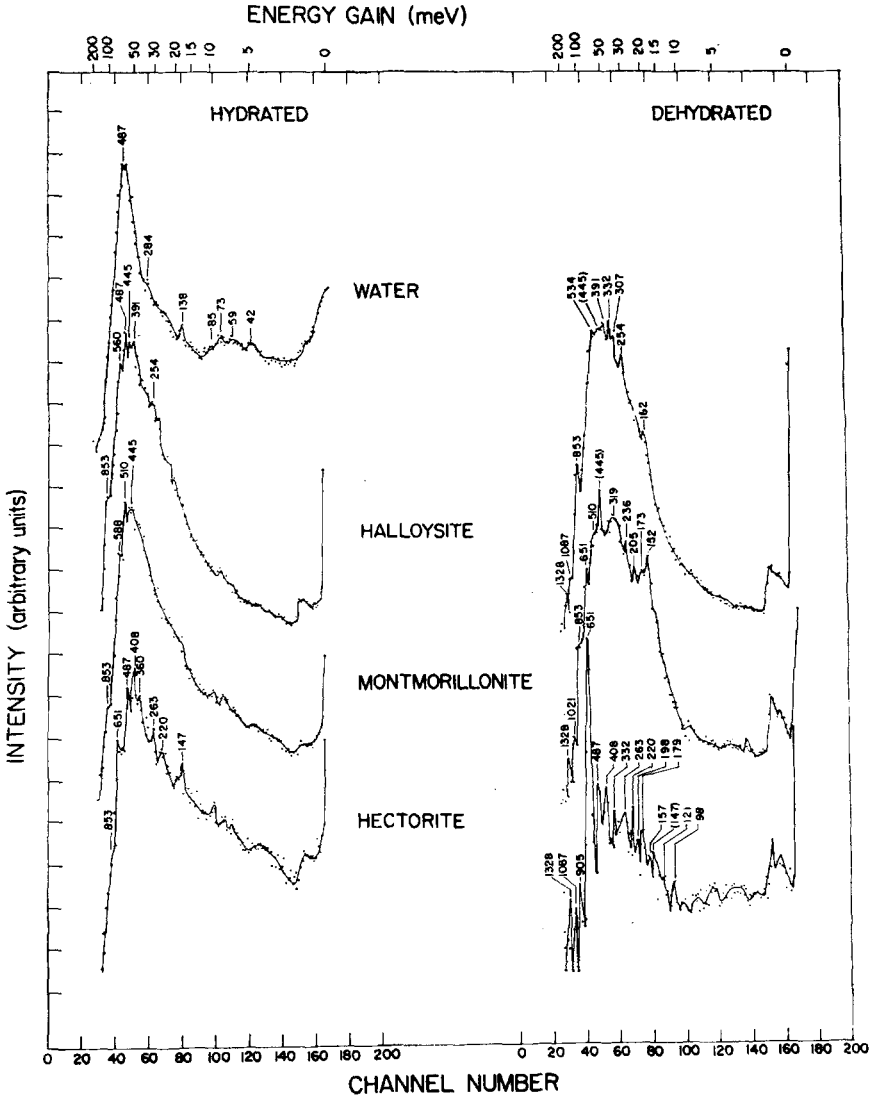


FIG. 7. Time-of-flight distributions for water, halloysite, montmorillonite, and hectorite.

montmorillonite gave spectra characteristic of dioctahedral, and hectorite a spectrum characteristic of trioctahedral, minerals. The structure below 100 cm^{-1} in the spectra of the dehydrated forms of montmorillonite and hectorite is an example of the behavior described above for finely divided materials.

https://doi.org/10.1346/CCMN.1966.0140132 Published online by Cambridge University Press

https://doi.org/10.1346/CCMN.1966.0140132 Published online by Cambridge University Press

TABLE 2.—SUMMARY AND COMPARISON OF FREQUENCIES OBSERVED BY NEUTRON INELASTIC SCATTERING

Kaolin	Dehydrated halloysite	Pyrophyllite	Dehydrated montmorillonite	Muscovite	Phlogopite	Hectorite	Talc	Serpentine	Amphibole
	1328		1328			1328			
1087	1087	1160	1021	1160	1160	1087		1240	1240
905	853	905	853	853	806	905	905	960	
				763					
								723	
		685							
		618	651	618	618	651	651	618	651
534	534	560							
		478	510	487	465	487	487	465	510
465		426		445	426				
375	391					408	391	408	375
	332	332		360	360	332		360	345
319	307	307	319				319	295	
263				273	273	263	284		273
245	245				245		254	254	
		228	236	236		220	228	228	
212		183	205	198	205	198	205	191	212
173		173	173	179	179	179	173	179	173
157	162		152		147	157		152	152
						121			114
		92			95	98			

TABLE 3.—COMPARISON OF FREQUENCIES OBSERVED BY INFRARED AND BY NEUTRON INELASTIC SCATTERING

Mineral	ν_{OH} Sidebands ν	$\Delta\nu_+$	ν	$\Delta\nu_-$	Direct IR observation	Neutron inelastic scattering
Muscovite*	ν_{OH} (fundamental) = 3628					
	4708	1080				1160±80
	4543	915	2707	921	928	853±50
						763±43
	4260	632	3003	625		618±33
	4200	572				
	4106	478	3117	511		487±23
					408	445±20
			3308	320		360±15
						273±11
	3874	246				236± 9
			3444	184	188	198± 7
					165	179± 6
					109	
Phlogopite*	ν_{OH} (fundamental) = 3708					
						1160±80
	4457	749	2854	854		806±47
	4371	663				
	4303	595	3110	598		618±33
	4204	496	3216	492		465±22
	4150	442				426±19
	4098	390	3316	392		360±15
	3998	290	3430	278		273±11
						245± 9
						205± 7
	3894	186	3528	180		179± 6
					151	147± 5
	3790	82			86	95± 3
Talc†	ν_{OH} (fundamental) = 3700					
						905±55
	4380	680	2990	710		
	4350	650	3030	670	670	651±34
	4210	510	3180	520	539	487±23
						391±17
						319±13
						284±11
						254± 9
	3920	220	3480	220		228± 8
						205± 7
						173± 6
	3780	80	3610	90		

* Data of Vedder (1964).

† Sideband data for talc were provided by A. L. Hallowell, Union Carbide Research Center, Tuxedo, New York. The direct IR frequencies are from the data of Farmer (1958).

https://doi.org/10.1346/CCMN.1966.0140132 Published online by Cambridge University Press

DISCUSSION

The NIS and IR spectra of $Mg(OH)_2$, $Ca(OH)_2$, and LiOH show a close correspondence in both the number and intensity of observed lines (Buchanan, Kinsey, and Caspers, 1962; Hexter, 1958; Safford, Brajovic, and Boutin, 1963; Safford and Lo Sacco, 1965) even though the former two have trigonal and the latter has tetragonal symmetry (Wyckoff, 1963, pp. 136 and 268). Because of this, the modes involved have been associated (except for some below 145 cm^{-1}) with unit-cell $(OH)^-$ vibrations, determined by local $(OH)^-$ cation coordination and symmetry, rather than by long-range order. No similar correspondence is observed between the spectra of $Mg(OH)_2$ and those of trioctahedral minerals, nor between the spectra of $Al(OH)_3$ and those of dioctahedral minerals. Thus, it is doubtful, in spite of previous efforts (Farmer, 1958), that there is a significant correlation between $(OH)^-$ vibrations in clay minerals and the corresponding hydroxides. In forming an alternative interpretation, it must be kept in mind that peaks below 900 cm^{-1} are expected to arise from vibrations of $(OH)^-$ groups as rigid units. In general, these are hindered oscillations and translations (including lattice modes). Cooperative stretching and bending vibrations of non-hydrogenous groups (such as cations and Si–O tetrahedra) which couple with $(OH)^-$ will also appear.

The most prominent features in the spectra of the trioctahedral series and the amphibole minerals are two peaks at 650–610 cm^{-1} and 510–465 cm^{-1}. These peaks are narrow, symmetric in shape, and have high relative intensity: features that characterize the motions involved as torsional components of $(OH)^-$ groups. The shapes indicate that, at best, only weak hydrogen bonding is involved (Pimental and McClellan, 1960, p. 125). The insensitivity of the peaks to long-range crystallographic order indicates that the torsional modes are only weakly coupled to lattice vibrations and are determined mainly by the charge, symmetry, and distances of the three nearest-neighbor cations. Indeed, as will be discussed later, these peaks are strongly shifted in the spectra of the dioctahedral analogs of the minerals, where a vacancy exists at one of the three cation sites and the symmetry and charge distribution in the neighborhood of the $(OH)^-$ groups are changed. The invariance of the peaks in the amphibole series, in which the Fe/Mg ratio changes considerably, is also in keeping with their assignment as torsional motions involving only the $(OH)^-$ groups. Although Mg^{++} and Fe^{++} have the same charge, and essentially the same ionic radius, the difference in mass would result in a shift in frequency for any vibrations involving a translation of an $(OH)^-$ ion against these cations.

There is a shoulder at 723 cm^{-1} in spectra of chrysotile that does not appear in those of the other trioctahedral clay minerals. When chrysotile is heated to 590°C, this shoulder disappears, but the torsional components at approximately 625 and 500 cm^{-1} are unaffected. This shoulder has been assigned to torsional vibrations of the outer $(OH)^-$ groups (hydroxyls located at the sur-

https://doi.org/10.1346/CCMN.1966.0140132 Published online by Cambridge University Press

face of the octahedral layers). It might be expected that, since there are more outer $(OH)^-$ groups than inner groups (hydroxyls in the plane common to the octa- and tetrahedral layers) that the former would produce the most intense peak. It is true that intensity depends upon the number of hydrogenous units participating in a given vibration, but other factors also contribute. For example, spectral peaks correspond to downward transitions between consecutive levels in a potential well, and their intensities are proportional to a Boltzmann population factor (Bauman, 1962, pp. 235 and 511). Such a factor can account for some, but not all, of the intensity difference. The remainder is most likely due to a broader frequency dispersion for the motions of the outer hydroxyls.

The torsional peak corresponding to the 650–620 cm^{-1} peak in the spectra of trioctahedral minerals appears at 900–850 cm^{-1} for their dioctahedral counterparts, and is lower in intensity in accord with a Boltzmann population factor. Indeed, the spectra of kaolinite at $T = 293°K$ and $T = 400°K$ show both that the intensity of the peak varies with the temperature dependence of such a factor and that a one-phonon neutron cross section is a valid approximation.* The weak lines that appear in the trioctahedral minerals at about 640 cm^{-1}, and in the trioctahedral minerals at 905–950 cm^{-1}, are attributed to divalent and trivalent impurities, respectively.

IR measurements support the assignment of the peaks as torsional oscillations. Vedder (1964) has reported a doublet at 579 cm^{-1} and 494 cm^{-1} in phlogopite on the basis of sum-and-difference side bands of the $(OH)^-$ fundamental. Corresponding torsional components were observed directly and in combination with the $(OH)^-$ fundamental in muscovite at 925 and 405 cm^{-1}, and these were observed to shift as expected for torsional modes in deuterated samples. Vedder and McDonald (1963) concluded that these represent motions with reference to a plane perpendicular to the cleavage plane, the higher-frequency component corresponding to a displacement of the proton perpendicular to, and the lower to a displacement in, the plane. The present data do not show a well-defined torsional component at 405 cm^{-1}. However, 405 cm^{-1} lies in a complex region of the spectra, and such a component could well be obscured. These authors have also pointed out that the coupling of librational and stretching motions of the $(OH)^-$ groups to lattice motions is expected to be weak. This is in keeping with the observations of the present experiment.

The difference in torsional frequency between the tri- and dioctahedral series again emphasizes that the torsional modes of the $(OH)^-$ groups are determined mainly by their coordination with nearest-neighbor cations. The orientation of $(OH)^-$ groups in trioctahedral minerals are nearly perpendicular to the cleavage plane, as would be expected from the symmetry of the electrostatic forces involved in the octahedral layers of these minerals. The

* This implies that $\theta_D \gg 400°K$ for kaolinite. The one-phonon approximation was assumed to be valid for all of the data of this investigation (for a discussion of this approximation, see Kothari and Singwi, 1959; and Pines, 1963).

https://doi.org/10.1346/CCMN.1966.0140132 Published online by Cambridge University Press

substitution of two trivalent for three divalent ions changes this symmetry to favor some intermediate angle between the perpendicular and the cleavage planes, and also leads to changes in polarization due to a decrease in cation–oxygen distances and an increase in hydrogen–oxygen distances. This argument was used by Bassett (1960) to explain the downward shift in frequency and the broadening of the $(OH)^-$ stretching fundamental in muscovite relative to phlogopite, and agrees with the present results, where the torsional peaks shift from ≈ 625 cm^{-1} in trioctahedral minerals to ≈ 925 cm^{-1} in the dioctahedral series. The tilt of $(OH)^-$ groups toward the cleavage plane in the dioctahedral minerals also permits a greater interaction with the oxygens of the tetrahedral layers. This, and the stronger coordination of the oxygens to the cations, would tend to tighten the coupling of $(OH)^-$ groups to the tetrahedral layer in dioctahedral, relative to trioctahedral, minerals.

The modes below 450 cm^{-1} are assigned to translatory vibrations of $(OH)^-$ groups. These will be optical or unit-cell modes of the type described in detail by Wickersham (1959), and acoustic modes. The former should appear as broader, less symmetric, and less intense peaks than the torsional maxima just discussed. The latter are the lowest-frequency modes and are the most sensitive to changes in long-range order. An acoustic mode should be characterized by a high-energy cutoff followed by a decrease in intensity toward zero frequency. In practice, the shape can be altered by the superposition of several acoustic branches, and by departures from the quadratic fall-off due to perturbations of the long-range order.

While torsional and stretching motions of $(OH)^-$ groups are not likely to couple strongly with the motions of an Si–O lattice, low-frequency translatory vibrations involving weaker force can mix with lattice vibrations (Vedder, 1964; Vedder and McDonald, 1963). A complete, normal-coordinate analysis of phase-frequency relationships would be needed to identify spectral lines that arise in this way, and to associate each with a specific mode of vibration. Saksena (1961) and Vedder (1964) have calculated vibrational frequencies that are IR active for a number of idealized chain and sheet Si–O structures, and a fair agreement exists between these frequencies and those obtained in this experiment. A more complete comparison must await a normal-mode calculation of the entire frequency distribution for all vibrations including Mg–O or Al–O, which can mix to a significant degree with the modes of tetrahedral layers. Certain observations can, however, be made concerning the low-lying frequencies. The di- and trioctahedral minerals show a correspondence in observed translational frequencies that is too large to be purely coincidental. A reasonable but speculative explanation for this correspondence is to assign these lines to $(OH)^-$ groups weakly coupled to the vibrations of the tetrahedral Si–O layers. Such frequencies would not be strongly mixed with Al–OH or Mg–OH modes, and thus would be mainly determined by the characteristics of the tetrahedral layers. The lowest-lying lines (≈ 240 cm^{-1}) in both the tri- and the dioctahedral series show the characteristic features expected for acoustic lattice modes with closely spaced high-frequency

https://doi.org/10.1346/CCMN.1966.0140132 Published online by Cambridge University Press

cutoffs. The spectra of antigorite-2 and pyrophyllite-2 are among the best examples. Both show the high-frequency cutoff followed by a nearly quadratic decrease in intensity toward zero frequency.

For trioctahedral minerals, there is little variation in peak intensity; but for dioctahedral minerals, peak intensities differ not only between mineral types, but also to a lesser degree between specimens of a given mineral. One must rule out the more usual sources of intensity variation; i.e. differences in scattering cross-section, differences in the number of hydrogenous units participating in the vibration, or differences in the density of the energy levels involved. The observed variations are too large to be accounted for by differences in cross-section or in the relative number of $(OH)^-$ groups bound in a similar manner. Differences in intensity due to differences in the density of levels implies an anharmonicity in the binding potentials of the $(OH)^-$ groups. Such anharmonicity, in turn, would cause shifts in frequency (Bauman, 1962, pp. 505) that are not observed.

In terms of the peak assignments just presented, the intensity variations observed with the dioctahedral minerals are attributed to variations in the degree of coupling of the $(OH)^-$ groups with the tetrahedral layers. The variations in coupling, in turn, are attributed to: (a) differences of the type described above in the coordination of the oxygens of $(OH)^-$ groups with nearest-neighbor cations and in the coordination of the protons of these groups to the oxygens of the tetrahedral layers, and (b) distortions of the tetrahedral layers that perturb OH–oxygen coordination. In an ideal layer silicate structure, the surface of each layer consists of an open hexagonal network of basal oxygens of Si–O tetrahedra. In most minerals, distortions arise because of a mismatch between the tetrahedral and octahedral layers. In talc, for example, the silica sheet is nearly fully extended and undistorted, but in muscovite the basal triads are rotated approx. 13° from the ideal position, (Radoslovich, 1960). The variations in peak intensities between different specimens of one mineral are usually smaller than those between different minerals. These variations are also attributed to small structural variations in the tetrahedral layers, in this case arising from variations in chemical composition or crystallinity.

CONCLUSIONS

No correspondence is found between the low-frequency motions of the $(OH)^-$ groups of the "gibbsite-like" and the "brucite-like" layers of clay minerals and those of pure gibbsite and brucite. Dioctahedral clay minerals have a characteristic frequency at 850–910 cm^{-1} associated with torsional oscillations that are determined primarily by nearest-neighbor cation coordination and symmetry. Trioctahedral minerals have similar, characteristic torsional frequencies at 620–650 cm^{-1} and 460–510 cm^{-1}. Frequencies that are attributed to translational motions of $(OH)^-$ units are found at frequencies below those of the torsional peaks. These are believed to be due to a coupling

https://doi.org/10.1346/CCMN.1966.0140132 Published online by Cambridge University Press

of $(OH)^-$ motions with the characteristic modes of Si–O tetrahedral layers. This assignment must be considered tentative. Clarification will require additional data, such as neutron diffraction measurements, to determine proton positions and "constant-Q" measurements (Brockhouse, 1961) of phase-frequency relations.

REFERENCES

BASSETT, W. A. (1960) Role of hydroxyl orientation in mica alteration, *Bull. Geol. Soc. Amer.* **71**, 449–56.

BAUMAN, R. P. (1962) *Absorption Spectroscopy*, J. Wiley, New York, 611 pp.

BROCKHOUSE, B. N. (1961) Methods for neutron spectrometry, in *Proc. Symposium Inelastic Scattering Neutrons in Solids and liquids*, International Atomic Energy Agency, Vienna, Austria **1**, 113–51.

BUCHANAN, R. A., KINSEY, E. L., and CASPERS, H. H. (1962) Infrared absorption spectra of LiOH and LiOD, *Jour. Chem. Phys.* **36**, 2665–75.

DANNER, H. R., SAFFORD, G. J., BOUTIN, H., and BERGER, M. (1964) Study of low-frequency motions in polyethylene and the paraffin hydrocarbons by neutron inelastic scattering, *Jour. Chem. Phys.* **40**, 1417–25.

EISENHAUER, C. M., PELAH, I., HUGHES, D. J., and PALEVOSKY, H. (1958), Measurements of lattice vibrations in vanadium by neutron scattering, *Phys. Rev.* **109**, 1046–51.

FARMER, V. C. (1958), The infrared spectra of talc, saponite, and hectorite, *Min. Mag.* **31**, 829–45.

GRAHAM, J., WALKER, G. F., and WEST, G. W. (1964) Nuclear magnetic resonance study of interlayer water in hydrated layer silicates, *Jour. Chem. Phys.* **40**, 540–50.

HEXTER, R. M. (1958) On the infrared absorption spectra of crystalline brucite $[Mg(OH)_2]$ and portlandite $[Ca(OH)_2]$, *Jour. Opt. Soc. Amer.*, **48**, 770–4.

HUGHES, D. J., and SCHWARTZ, R. B. (1958) *Neutron Cross Sections*, 2nd ed., BNL-325, Brookhaven National Laboratory, Upton, New York.

KOTHARI, L. S., and SINGWI, K. S. (1959) Interaction of thermal neutrons with solids, *Solid State Phys.* **8**, 109–90.

PIMENTAL, G. C., and MCCLELLAN, A. L. (1960) *The Hydrogen Bond*, W. H. Freeman, San Francisco, 475 pp.

PINES, D. (1963) *Elementary Excitation in Solids*, W. A. Benjamin, New York, 299 pp.

RADOSLOVICH, E. W. (1960) The structure of muscovite, $KAl_2(Si_3Al)O_{10}(OH)_2$, *Acta Cryst.* **13**, 919–32.

SAFFORD, G. J., BRAJOVIC, V., and BOUTIN, H. (1963) in Investigation of the energy levels in alkaline earth hydroxides by inelastic scattering of slow neutrons, *Jour. Phys. Chem. Solids* **24**, 771–7.

SAFFORD, G. J. and LO SACCO, F. J. (1965) A study of the low-frequency motions of LiOH by neutron inelastic scattering, Submitted to *Jour. Chem. Phys.*

SAKSENA, B. D. (1961) Infrared absorption studies of some silicate structure, *Trans. Faraday Soc.* **57**, 242–58.

STUBICAN, V. and ROY, R. (1961) A new approach to assignment of infrared absorption bands in layer-structure silicates, *Zeit. Krist.* **115**, 200–14.

VEDDER, W. (1964) Correlations between infrared spectrum and chemical composition of mica, *Amer. Min.* **49**, 736–68.

VEDDER, W. and MCDONALD, R. S. (1963), Vibrations of the OH ions in muscovite, *Jour. Chem. Phys.* **38**, 1583–90.

WICKERSHEIM, K. A. (1959) Infrared absorption spectrum of lithium hydroxide, *Jour. Chem. Phys.* **31**, 863–9.

WYCKOFF, R. W. G. (1963) *Crystal Structures*, 2nd ed., **1**, Interscience Publishers, New York, 467 pp.

https://doi.org/10.1346/CCMN.1966.0140132 Published online by Cambridge University Press